Precision measurement of the growth rate and mechanism of ibuprofen {001} and {011} as a function of crystallization environment

T. T. H. Nguyen, R. B. Hammond, K. J. Roberts*

Institute of Particle Science and Engineering, Institute of Process Research and Development, School of Process, Environmental and Materials Engineering, University of Leeds, Leeds, LS2 9JT, Leeds

I. Marziano, G. Nichols

Pfizer Worldwide Research and Development, Sandwich, CT13 9NJ, UK

(*) Corresponding author's email: K.J.Roberts@leeds.ac.uk

Abstract

The crystallisation of ibuprofen under diffusion-limited conditions measured as a function of supersaturation, solvent (95% ethanol/water, ethyl acetate, acetonitrile and toluene) and reactor scale is examined. Measurement of solubility as a function of temperature reveals less than ideal behaviour, consistent with strong solute-solute interactions, particularly in the case of acetonitrile. The crystal growth rates of the {001} and {011} faces of spontaneously nucleated crystals are precisely measured in-situ using optical microscopy revealing that their respective growth rates increase with increasing supersaturation to different extents, depending on the solvent type, with concomitant impact on the crystal habit. The measured aspect ratios, as a function of supersaturation, are generally higher at the 15 mL than the 0.5 mL scale size. Analysis of the growth rates versus supersaturation is consistent with a 2-D surface nucleation (Birth and Spread) model for both faces and at both scale sizes. The growth rates of the {001} and {011} faces exhibit much less growth rate dispersion when compared to literature data for a stirred batch crystallizer.

The data is rationalized by examining the surface chemistry of the growing faces revealing, e.g. that polar protic solvents inhibit the growth rate of faces containing available binding sites for hydrogen bonding formation, such as carboxylic acid groups.

Key words: Crystallisation, ibuprofen crystals, growth rate measurements, optical microscopy, image analysis, crystal morphology, solvent induced habit modification, re-entrant morphological features, science of scale, interfacial kinetics characterisation, growth rate dispersion, solution structure and ideality.

1 Introduction

Crystallisation is an important purification, separation and pre-formulation process in the pharmaceutical and fine chemical process industries. It is the primary method applied for the intermediate and final stage production of a wide range of materials from inorganic compounds to high value-added organic materials such as active pharmaceutical compounds and specialty chemicals. However, the anisotropic nature of a crystalline material combined with the complex molecular and crystal chemistry of many specialty compounds can conspire to produce a high degree of variability in the physical properties of crystalline products. This can, in turn, lead to significant changes in product quality, i.e. impacting upon stability, bioavailability, processability, crystallinity and/or purity. In order to isolate the crystals which exhibit the desired physical properties, the fundamental process of crystal growth and its associated kinetics need to be understood, characterised and controlled. Previous studies in this area have mostly presented measurements of growth rates of single crystal seeds grown at comparatively low supersaturations [1-6]. Alternatively, measurements have been made of the growth rate of a population of crystals as prepared under crystallisation reactor environment conditions e.g. through the measurement of the characteristic dimensions (such as length, width, and equivalent diameter etc.) associated with the growth of the crystals [7-14]. Linking these two, quite distinctive, sets of measurements is a challenge mindful of the quite different hydrodynamic environments involved. For example in the former case whilst measurements are made on the individual growth faces, the influence imposed either by the hydrodynamic environment associated with the measurements or by the selection of the specific seeds [15] for the studies is not really defined. Similarity, in the latter case, it is hard to extract out the kinetics associated with the growth of the individual habit faces. Within this overall context, there have been

surprisingly limited kinetic studies on the growth of the individual faces of spontaneously-nucleated crystals as prepared under diffusion-limited growth conditions in stagnant solutions. Such measurements are helpful in that they provide baseline crystal growth kinetic data from which the impact of e.g. agitation and mixing can be subsequently assessed. Additionally, few detailed studies of the growth rates of single crystals have been published which focused on growth-rate dispersion [16-18] particularly those which highlight variability of the growth rate of individual crystals within a population. A significant factor in the scarcity of research resulting from investigations into the growth rates of single crystal growth perhaps lies in the lack of rapid and routine experimental methodologies for studying these aspects. This, perhaps, reflects the fact that the most common techniques available for crystallisation monitoring are intended for use at the larger scales and are aimed at measuring what is defined as the crystal size distribution. In such cases size is usually represented by an average values for growth rates based on an assessment of a crystal population e.g. using focused beam reflectance measurements (FBRM) [19-21], rather than face-specific growth rates as measured for batches of individual crystals. For example, most of commercial particle size instruments calculate the crystal 'size' in terms of a volume equivalent diameter (D_{volume}) where:

$$D_{volume} = \left[\frac{6}{\pi} V_{particle}\right]^{1/3} \quad (1)$$

Providing equant particles are being measured this is a reasonable charactersisation of particle size but for crystals exhibiting anisotropic morphologies, the results can be confusing (see Figure 1).

Figure 1 Schematic diagram showing hypothetical particles with different shapes whilst still having the same volume equivalent diameter highlighting the importance of measuring shape-dependant crystal growth rates: (a) 100μm diameter sphere which has the same volume as (b) cube (with the size of an edge = 80.6 μm), (c) a rectangular needle (20 μm x 25 μm x 1047 μm) and (d) a very thin plate (200 μm x 262 μm x 10 μm).

A fundamental evaluation of the growth kinetics must be based on the growth rates of individual faces [22] for which a detailed understanding of the crystal shape is a crucial factor in growth rate determination.

The above scenario is addressed in this study through the measurement of the growth rates of the individual crystal faces of the pharmaceutical compound ibuprofen as a function of its solution crystallisation environment from which the likely interfacial crystal growth mechanisms involved were characterised.

RS-ibuprofen (2-(4-isobutyl-phenyl) propionic acid), $C_{13}H_{18}O_2$ M = 206.28g/mol, melting point (77-78^{o}C) is a non-steroidal anti-inflammatory drug (NSAID) that has been used to relieve pain, cold, fever and inflammation. This material crystallizes in a monoclinic crystal structure with space group $P2_1/c$ in a tetramolecular unit cell with unit cell dimensions a = 14.667Å, b = 7.886 Å, c = 10.730 Å, β = 99.3628^{o}, Z = 4 [23, 24]. The crystal packing manifests centrosymmetric hydrogen-bonded dimers [23] (Figure 2). Dudognon, et al. [25] have shown an evidence for a new crystalline form of racemic ibuprofen as prepared under quite extreme conditions, i.e. at least 60^{o}C below the glass transition temperature Tg (Tg = 228K). However, the full crystal

structure for this form has not yet been published. Crystal of the known structure of ibuprofen to exhibit [26, 27] three dominant crystal habit faces; {100}, {001} and {011} and the crystals of racemic ibuprofen exhibit different crystal habits as a result of varying the crystallisation conditions. This material mostly has a plate-like crystal morphology dominated by a large {100} face with smaller {001} and {011} side faces. Despite the fact that changes in crystal habit have been reported many times [2, 26, 28-34], detailed studies of growth kinetics for this material have been surprisingly limited. Rashid, et al. [11] studied growth rates of ibuprofen crystals grown from ethanol by adding size proportional growth (SPG) seed crystals to an isothermal non-nucleating batch crystallization vessel and sampling the resultant crystals during the batch. They found that ibuprofen crystallising from ethanol exhibits significant growth rate dispersion. This phenomenon refers to the fact that the growth rates of crystals of the same material and size, when exposed to identical conditions of supersaturation, temperature and fluid dynamics, do not subsequently grow at the same rate [17, 35, 36]. Cano, et al. [2] measured the growth rates of the {100}, {001} and {011} faces in a single ibuprofen crystal using a crystal-growth flow cell. During these measurements, a crystal was secured within the cell with the crystal faces of the seed crystal being oriented with respect to the solution flow in order to obtain reproducible growth conditions at relative supersaturation (σ) of 0.013. However, this work did not provide information on the growth rates for spontaneously nucleated crystals nor were the variations in the crystal growth rates between different crystals studied. Reflecting this, this paper reports the measurement of the solution solubilities and crystal growth rates of the associated {001} and {011} surfaces of self-nucleated single (RS)-ibuprofen crystals in stagnant solutions at two scale sizes; 0.5ml and 15ml, as a function of solvent (95% ethanol/water, ethyl acetate, acetonitrile and

toluene) and relative supersaturation σ from 0.55 to 1.3. From this, the interfacial growth mechanisms of these faces with this range of supersaturation were characterised.

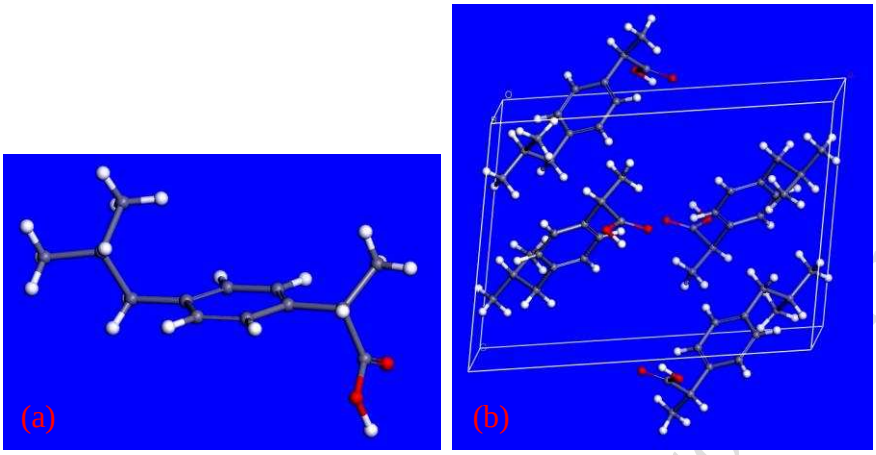

Figure 2 Molecular diagram showing (a) molecular structure and (b) intremolecular packing in the crystallographic unit cell ibuprofen molecule

2 Crystal growth rates and kinetics

2.1 Growth rate expressions

There is broad agreement in the literature that there are three main methods [37] to express the crystal growth rate:

2.1.1 Face growth rate

Face growth rate v_{hkl} (m/s) is the velocity of movement forward of the crystallographic faces in a direction perpendicular to a face (hkl), which can be measured on individual crystal faces over time using a microscope thus:

$$R_L = \frac{\Delta L}{\Delta t} \quad (2)$$

where ΔL is the distance of movement forward of a crystal surface (hkl) in a period of time Δt

Growth rates expressed in this way can be related to the different interfacial crystal growth mechanisms and models.

2.1.2 Overall mass growth rate

Overall mass growth rate, R_G (kg/m^{2}s), is expressed for the average growth rate of whole population of crystals and has often been used for calculating product yields and for design purposes for optimizing batch crystallisation processes;

$$R_G = \frac{1}{A_c}\frac{dM_c}{dt} = \frac{\rho_c}{A_c}\sum v_{hkl}A_{hkl} \quad (3)$$

where M_c is the mass of crystal; A_C is the surface area of whole crystal; and A_{hkl} is the area of face hkl, v_{hkl} is the face growth rate and A_{hkl} is the area of the faces on a crystal

2.1.3 Overall linear growth rate

Overall linear growth rate, G, (m/s or μm/s), is the rate of change of the crystal's characteristic dimension, L, has dimensions of velocity, which depends on the specific characteristic dimension used in the definition:

$$G = dL/dt \quad (4)$$

G and R_G can be related as follows:

$$R_G = \frac{1}{A_C} * \frac{dM_C}{dt} = \frac{1}{\beta.L^2}\frac{d(\alpha\rho_c L^3)}{dt} = \frac{3\alpha\rho_c}{\beta}\frac{dL}{dt} = \frac{3\alpha\rho_c}{\beta}G \quad (5)$$

$$M_C = \alpha.\rho_c.L^3 \quad (6)$$

$$A_C = \beta.L^2 \quad (7)$$

where ρ_c is the density of crystals, α is the volume shape factor and β is the crystal surface shape factor. If crystals are spherical or cubic then β/α = 6

$$R_G = \frac{1}{2}\rho_C.G \quad (8)$$

It is important to define this dimension when using this expression. L is often defined with respect to the technique used in its measurement.

The latter expression is commonly applied within population balance theory models which relates the crystal size distribution (CSD) to the crystallisation kinetics [38] thus:

$$\frac{\partial(nV)}{\partial t} + \frac{\partial(GnV)}{\partial L} = 0 \quad (9)$$

where n is the population density per unit volume, V is the total suspension volume of the crystallizer, G is the linear growth rate, L is the crystal size and t is the time

Whilst the population balance model is helpful in defining crystallisation kinetics, it relies on empirical parameters for the characteristic size. Recently, 2D [8, 13, 14, 39, 40] and morphologically based [41-43] population balance models have been developed. The latter case offers a significant improvement in that the multi-dimensional characteristic lengths are defined with respect to the growth rates of the individual crystal habit faces. This provides a more 'first-principle' model and one, in particular, that takes into account the morphology of the growing crystal. The utility of incorporating morphological data into measurements of the characteristic length of crystals has been demonstrated by Penchev [44] who used morphological analysis to decompose crystal size data of L-glutamic acid obtained in-situ using ultrasonic spectroscopy into a sub-set of characteristic lengths based on the measurements of the three growth forms (001), (111) and (011) for which their individual interface kinetic mechanisms were determined. Nowadays, in-process data mostly uses FBRM instrumentation [19-21] which measures only the chord length distribution which can be challenging to extract 'first-principles' face-specific kinetics [45].

Measurements of the growth rates of crystal populations, usually involve seeding within the metastable zone. However, the process can itself provide variability in the measured growth rates [46-48] depending on the seed preparation techniques adopted and/or the size fraction selected and/or the seed concentration. The latter reflects the impact of these variables on the secondary nucleation process highlighting the value of having base-line face-specific growth rate studies on spontaneously nucleated crystal prepared under diffusion-controlled conditions.

It is well-known that crystals of the same material and size, when exposed to seemingly identical crystallisation conditions, do not always grow at the same rate; a phenomenon known as growth rate dispersion (GRD) [18, 35, 36, 49]. Whilst size dependent growth (SDG) [50] relates to crystals of different sizes growing at different rates, GRD is a phenomenon where similar sized crystals grow at different rates under apparently identical conditions of supersaturation, temperature and hydrodynamics. Variations of growth rate of the uniform sized crystals affects the CSD of the product crystals and hence the product quality. The studies of the physical mechanisms underlying of GRD have resulted in the development of three models which provide a basis for further analysis of experimental data: the constant crystal growth model (CCG) [49]; the random fluctuation model (RF) [51]; and the 'fast-growers', 'slow-growers' model (FGSG) [52].

2.2 Crystal growth rate measurement techniques

There have been various techniques for in-situ crystallisation process monitoring and for measurement of the crystal growth rates. However, different systems and applications require the use of different methods. For example, transmission light optical microscopy is often used for the determination of the growth rates of individual crystal faces, while interference contrast, phase

contrast or interferometric incident light microscopies are usually used for measuring step velocities, particularly in cases where the step height and spacing is small. Optical microscopy techniques together with a video imaging and image analysis software have also been used to derive growth rate data [2-5, 35, 53].

This approach has been enhanced through the use of stroboscopic techniques together with computational methods for analysis of crystallisation processes within agitated batch vessels [7-10]. High speed imaging processes has also been used to capture high resolution images on-line and perform real-time, in situ particle analysis [10, 13, 14, 54]. Other methods reported for growth rate determination include atomic force microscopy (AFM) [55-59], Michelson interferometry [60-64] and laser polarization-interference techniques [65].

2.3 Assessment of the interfacial growth mechanism for growth rate data

The growth rate of a crystal face is dependent on its underlying growth mechanism [66], which, in turn, is governed by the nature of the molecular attachment of solute molecules onto the growing crystal surface [67]. There are three generally accepted mechanisms for crystal growth each of which reflects on a particular range of supersaturation (Figure 3).

2.3.1 Screw dislocation (BCF) mechanism

According to the BCF mechanism (Burton, Cabrera and Frank) [68], at low supersaturation, the crystal growth process occurs via 2-dimemsional diffusion of solute molecules over the crystal surface. The incorporation of growth units onto the stepped surface provided by protrusion of dislocations leads to the formation of a growth spiral over the crystal surface creating a permanent source of growth steps at the crystal surface. As such, it readily allows the attachment

of growth units onto the surface hence facilitating its subsequent growth and development. The resulting growth rate expression is given by:

$$R_{hkl} = A\sigma^2 \tanh(\frac{B}{\sigma}) \quad (10)$$

where σ is relative supersaturation and A and B are complex temperature-dependent constants.

2.3.2 Birth and Spread mechanism (B&S)

In the absence of a permanent source of surface steps, the growth rate is limited by 2D nucleation through the B&S mechanism [69, 70]. In this, at higher supersaturation nucleation can occur without the need for the existence of the edge and kink sites provided in the BCF mechanism and this can take place anywhere on the crystal surfaces. Surfaces growing with this mechanism develop through the nucleation (birth) and growth (spread) a monolayer. After nucleation, further molecules can absorb and integrate into the existing monolayer thus enabling it to spread over the surface followed, in turn, by further 2D nucleation events when the surface layer has fully spread over the surface. In this mechanism, the relationship between the face growth velocity and supersaturation can be expressed through a largely exponential dependence on supersaturation:

$$R_{hkl} = A_1\sigma^{5/6} \exp(\frac{A_2}{\sigma}) \quad (11)$$

Where A_1 and A_2 are system-specific constants

2.3.3 Continuous growth (rough interfacial growth) model:

At high supersaturation, the growth interface undergoes surface roughening providing through this abundant sites for surface integration with a lot more step and kink sites thus resulting in a much higher growth rate [71]. Within this region, the energetics of growth unit attachments are the same regardless of the direction of solute adsorption producing morphologies which result in

the loss of a coherent set of surface terraces and well-defined crystal habit planes for growth. In extreme cases this can lead to the formation of a hopper [72] or dendritic [73] crystal forms. Multi-nucleation can also take place within the same spatial region resulting in formation of intergrowths, inter-crystal aggregates as well as twining [74] and spherulitic [73] growth forms. In this region, growth is expected to proceed via a linear dependence of the growth rate on supersaturation:

$$R_{\mathrm{hkl}} = \mathrm{A}\sigma \tag{12}$$

Where A is a constant

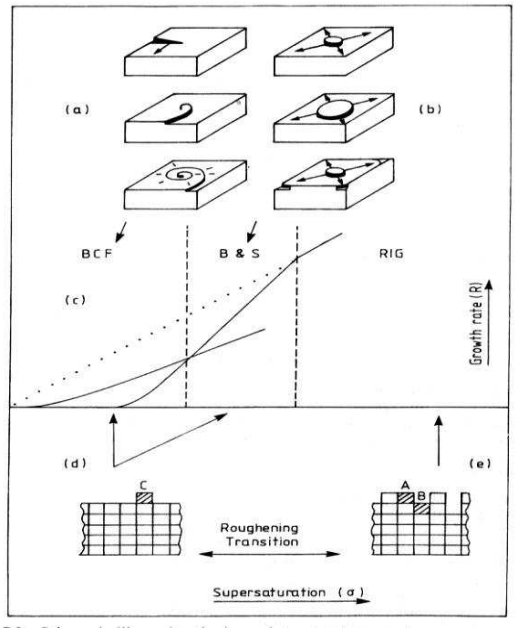

Figure 3 Schematic diagram illustrating the different crystal growth rate mechanism place at the crystal/solution interface, involving BCF (a) B&S (b) together with the expected correlation of these crystal growth mechanisms as a function of solution supersaturation (c) and the transition between stable growth on smooth surface to unstable growth at the roughened crystal/solution interface ((d) and (e)). Reproduced with the permission of Journal of Physics D: Applied Physics, 1993. 26(8B): p. B7. [75]

For a given material, crystal symmetry may give rise to different surface chemistry for each of the unique crystal forms. This can, in turn, lead to different surface bonding configurations being associated with the growth process for the different habit faces. Hence, the interfacial growth kinetics mechanism prevalent for a given crystal face may not be the same as that involved on another surface. In addition, the supersaturation dependence of the growth rate can also be expected differ between one crystallographically unique plane and another. Thus, full control over the particle properties resulting from a crystallisation process ideality requires the measurement of full kinetic data for each of the dominant crystal habit faces.

3 Materials and methods

3.1 Materials

Ibuprofen (melting point 75-77^{o}C, purity ≥ 98%) was obtained from Sigma Aldrich and Tokyo Chemical Industry UK Ltd. The solvents used were: 95% ethanol/water (the azeotropic composition of a binary mixture of ethanol and water) from Sigma Aldrich, ethyl acetate 99.5% Acros Organics, acetonitrile 99.9% from LC-MS and anhydrous toluene 99.8% from Sigma-Aldrich.

3.2 Experimental apparatus details

3.2.1 Solubility determination

An attenuated total reflection (ATR) UV/Vis spectroscopy system comprising a Varian Cary 50 spectrophotometer equipped with a 6.35mm diameter sapphire crystal titanium sheathed ATR probe from Hellma Analytics (http://www.hellma-analytics.com/) was employed for solubility determinations of solutions of ibuprofen in all solvents except toluene where gravimetric methods were used. The UV/Vis spectrophotometer operated over the wavelength range from 240 - 1100nm and was optimal for the direct measurement of strongly absorbing solutions (high

solubility solutions) where standard transmission probes cannot be used. This measurement approach had further advantages that: it involved no sampling; the solutions did need not be diluted; it was applicable for the measurement of high-solids content slurries on-line; and it was easy to set up with a flexible fiber-optics connection to the probe.

Unfortunately the UV/Vis depth of penetration for the ATR probe for the toluene system at the critical angle increases to infinity at 319 nm [76] and hence this technique could not be used for ibuprofen solubility measurements in toluene. In this case, the solubility was determined using gravimetric methods.

3.2.2 Growth rate measurements

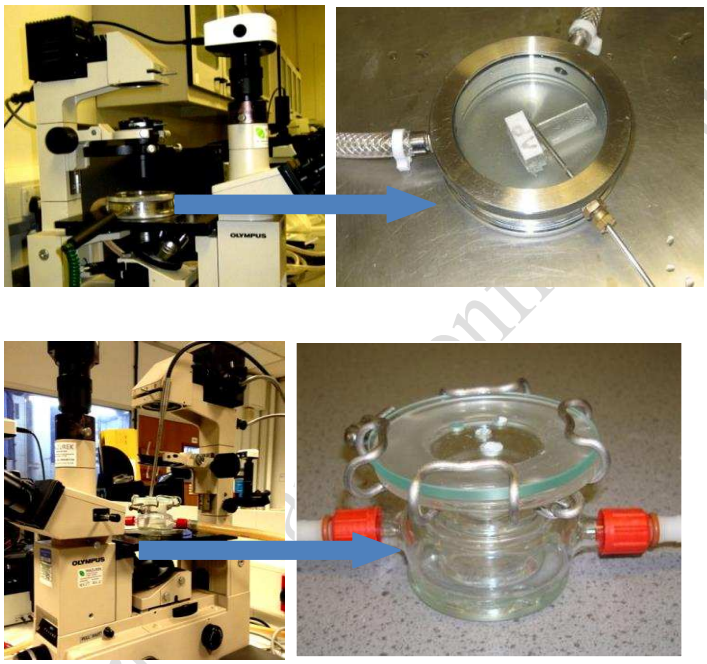

Figure 4 Crystallization system set up for measurement of crystal growth rate in a small scale cuvette 0.5ml (above) and in a larger scale jacketed-vessel15ml (below)

The growth rates for the {001} and {001} habit planes for individual single crystals as function of the growth solvent used and the solution supersaturation were measured at two scale sizes: a

0.5ml and 15ml. The crystallization setup employed for this comprises an inverted optical polarizing microscope (Olympus Optical IMT-2 or Leica/ Leitz DM IL 090-131-002) integrated with a CCD Lumenera Infinity 3.3 megapixel camera, a PC with image capture and image analyze software (http://www.lumenera.com/products/microscopy-cameras/index.php) to capture crystal images during the growth process. The crystallisation vessels (Figure 4) comprised of:

- A UV cuvette cell 0.5ml (54 x 10 x 1 mm) submerged in a shallow tank of water whose temperature was controlled by a Haake F3 recirculation bath.
- A 15ml jacketed vessel (34 (mm) ID diameter x 17(mm) height), with flat optical glass dics at the top and the bottom connected to a Huber ministat chiller. The jacketed vessel was equipped with an ATR UV/Vis spectrometer immersion probe to monitor the solution concentration and hence the level of supersaturation during crystallisation.

3.3 Experimental techniques

3.3.1 Solubility measurements

A set of saturated solutions with excess, suspended solids of (RS)-ibuprofen in various solvents were prepared in 20ml vials and put in a shaker unit (MaxQ 2000 Barnstead/Lab-line) maintained at constant temperature using a Julabo F25 re-circulating bath. The vials were agitated for 24 hours then allowed to settle for 6 hours to ensure all solids were separated from the saturated solvent. The saturated solutions were separated from solid phase for solubility measurement.

(a) ATR UV-Vis spectroscopy method: Calibration curves were obtained by scanning a series of known concentrations of ibuprofen in solvents over the wavelength range from 300 to 250nm. Solutions of ibuprofen of known solute concentration were analyzed by UV-Vis spectroscopy at the maximum absorbance in UV region (λmax = 264 nm) [77]

corresponding to the electron transition associated with the benzene ring. Saturated solutions at different temperatures were also scanned to obtain absorbances and hence the solubility of ibuprofen at various temperatures was determined from the calibration curve.

(b) Gravimetric method: One gram of saturated solution at different temperatures 15^{o}C, 20^{o}C, 25^{o}C, 30^{o}C, 35^{o}C was withdrawn and transferred to vials, the solvents were then allowed to evaporate at room temperature for approximately one week until the remaining mass of solid-material was constant with time and then the solubility, expressed in gram of solutes/gram of solvent, was calculated by the equation (g/g$_{solvent}$):

$$s = \frac{m_{solid}}{1-m_{solid}} \quad (13)$$

3.3.2 Thermal analysis measurements

DSC data was measured using a Mettler DSC 820 differential scanning calorimeter. Each sample was heated from 25 to 85°C at 5^{o}C/min in aluminum pans under nitrogen atmosphere. The onsets of the melting points and enthalpies of fusion obtained from the integration of the corresponding exothermic peaks were determined using STAR^{e} software.

3.3.3 Growth rate measurements {001} and {011} faces

RS-ibuprofen solutions were prepared by dissolving solute in ethanol 95% (1.4g/ml), ethyl acetate (1g/ml), acetonitrile (0.4g/ml) and toluene (1g/g). For the 0.5ml scale, a pipette was used to transfer the prepared solution into the cuvette cell which was sealed and fixed to the bottom of the water tank. For the 15ml scale, the prepared solution was transferred into the vessel.

The ibuprofen/solvent solutions were heated to 50^{o}C to completely dissolve all ibuprofen crystals, then the solutions were cooled down to a constant temperature such as 20, 23, 25 and 27^{o}C to maintain a specific supersaturation. At the 15ml scale this was monitored using ATR UV/Vis

spectroscopy and the system was monitored until crystals were found to appear. Image analyze software was used to capture a temporal sequence of images of the crystals as they developed.

3.4 Data analysis

3.4.1 Solubility

The ideal solubility of a crystalline material in a solvent was calculated by:

$$\ln X = \frac{\Delta H_{fus}}{R}\left(\frac{1}{T_{fus}} - \frac{1}{T}\right) \tag{14}$$

where X is mole fraction of the ideal solubility of the solute; ΔH_{fus} is molar enthalpy of fusion of the pure solute; T_m is melting point (K); T is the solution temperature (K). The assumption was made that the heat capacity difference between the melt and the solid state, both at solution temperature, were independent of temperature and negligible.

From the experimental determination of the solubility data for ibuprofen in solvents, the enthalpy and entropy of dissolution were calculated using the van't Hoff equation:

$$\ln X = -\frac{\Delta H_{diss}}{RT} + \frac{\Delta S_{diss}}{R} \tag{15}$$

where X is the mole fraction of solute in solution and ΔH_{diss} and ΔS_{diss} are the enthalpy and entropy of dissolution, respectively;

According to Raoult's law, the activity coefficient of the solute in the saturated solution, γ_i^{sat}, is defined as the ratio of the ideal and the experimentally measured solubilities at a given temperature:

$$a_i^{sat} = x_i^{sat}\gamma_i^{sat} \tag{16}$$

where a_i^{sat} is the activity of the solute i in the saturated solution and x_i^{sat} denotes the mole fraction experimental solubility. For an ideal solution, $a_i^{sat} = x_i^{sat}$.

The calculated activity coefficients (γ) were fitted with respect to its variation with temperature by:

$$\ln\gamma = aT + b \quad (17)$$

3.4.2 Crystal growth rate determinations

The growth rates of the {110} and {011} faces were measured using two different methods as shown in Figure 5whereby measurements are made of the:

- Length of a line from the centre of the crystal and perpendicular to the projection of the crystal edges for (001) or (00-1) & (011) or (0-11) or (01-1) or (0-1-1) faces (assuming crystals are symmetric).
- Separation distance between two opposite parallel faces of crystals which is then divided by two.

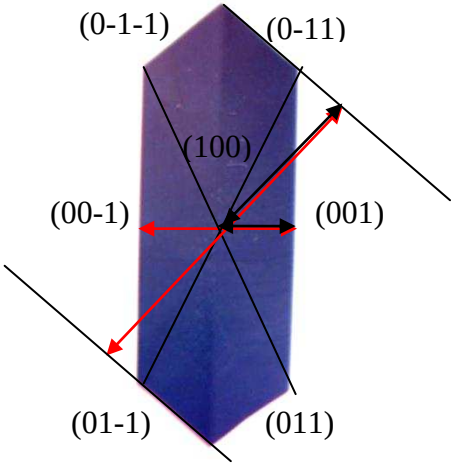

Figure 5 Image of crystal with overlaid annotations highlighting the methodology for the measurement of growth rate of the individual faces

Due to that fact that 'as grown crystals' tend not always to be symmetric, the second method can be a more accurate and is also easier to use than the first one. Assuming the crystal is lying flat on one of its dominant {100} faces, the in-plane measurements were geometrically corrected with the aid of the program MORANG [78] to allow for the tilt of the {001} and {011} planes (80.64^o and 84.42^o respectively) with respect to the sample's {100} habit plane. The growth rates of the individual crystal faces were determined by capturing images at chosen time-intervals (typically from 1-10 minutes, depending on the magnitude of the growth rate concerned). The growth normal distance from the center of the crystals to the faces as a function of time was calculated. The growth normal projection with time was found to be linear reflecting only a slight depletion of the solute concentration. This was used to assess the individual growth rates as a function of habit plane. Mean growth rates, together with their standard deviations, were calculated from the samples measured, typically between five to eight crystals under similar conditions. The linear growth rate of individual crystal surfaces was estimated from the increase of the distance from center to the face during each time interval. The coefficient of variation (CV_V) for the growth rate of each crystal face in each solvent and two scale-sizes was calculated by:

$$CV_v = \frac{SD}{R} \tag{18}$$

where SD is the standard deviation and R is the mean growth rate of the crystal faces for single crystals or the mean size of volume based distribution for a population of crystals in agitated vessel.

3.4.3 Growth mechanism

The growth mechanism was investigated through the use of user-defined fitting function using the two appropriate growth kinetic models, Birth and Spread (equation 4) and BCF (equation 5) expected for facetted growth and the results compared to evaluate which model gave the better fit. The data fitting was carried out using the nonlinear curve-fitting options in Origin [79]. The quality of regression can be measured by the coefficient of determination R^2. In this, if the adjusted R-square were found to be close to 1, the relationship between supersaturation and mean growth rate was regarded as being very strong, i.e. showing a high degree of confidence in the regression model. In contrast, when adjusted R^2 is negative this implies that the data fit to the model is poor [79].

3.4.4 Surface chemistry analysis

Molecular scale models of the crystal surfaces were simulated using Accelrys Material Studio [80]. From this, the changes in the measured crystal growth rates for the {001} and {011} surfaces with growth environment were rationalised through surface chemistry analysis, through which the characteristics of these surfaces (e.g. hydrophobicity, polarity or hydrogen-bonding propensity) were examined and the relative binding interactions between solvent and solute and the associated inter-molecular interaction involved on specific growing faces were analyzed.

4 Results and discussion

4.1 Solubility and solution behaviour

Full details of UV Vis calibration method and the gravimetric studies are given in section S1 within the supplementary materials.

The onset of melting point temperature and heat of fusion (ΔH_{fus}) were found to be 75.25^{o}C and 25.3KJ/mol respectively. The solubility curves of ibuprofen in ethanol, ethyl acetate, acetonitrile

and toluene solvents in both conventional and van't Hoff coordinates together with the ideal solubility relationship are given in Figure 6. These data are summarised in table 1.

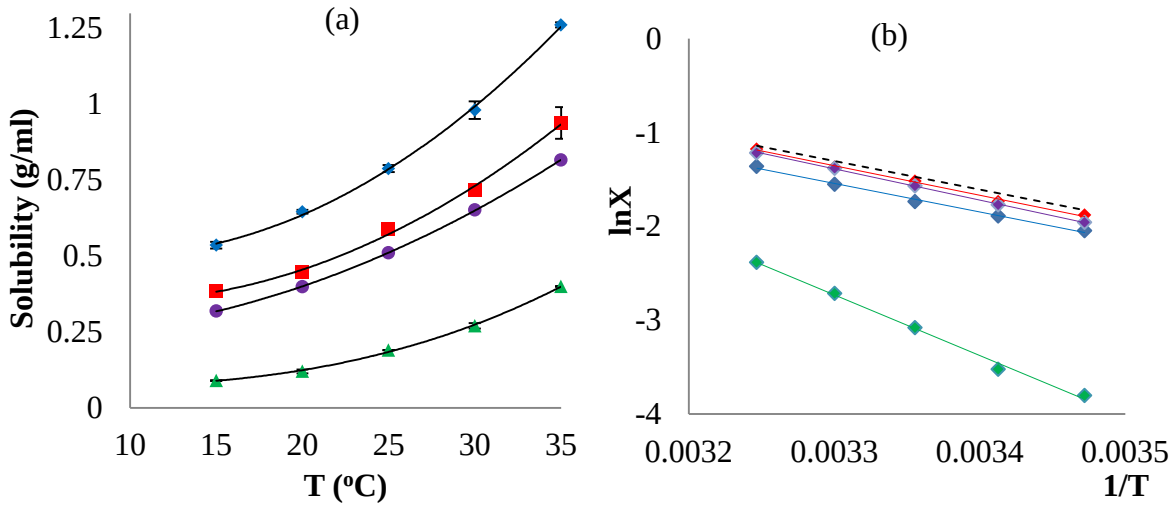

Figure 6 Solubility of ibuprofen in ethanol 95% (blue), ethyl acetate (red), acetonitrile (green) and toluene (purple) at temperatures from 15-35°C (a) together with plots of 1/T versus lnX of the ideal solubility (the dotted line) and the real solubility (solid lines) of ibuprofen in the same solvents (b)

Table 1 Enthalpy of dissolution, ΔH, and entropy of dissolution, ΔS, of ibuprofen in ethanol, ethyl acetate, acetonitrile and toluene together with calculated activity coefficient and temperature dependence fitting parameter. Logarithm of activity coefficients of ibuprofen in solvents as a function of saturated temperature (equation 11)

Solvents	Ethanol 95%	Ethyl acetate	Acetonitrile	Toluene
Dipole moment	1.69	1.78	3.92	0.36
Solubility (mg/g) 20^{o}C	822.8	502	152.7	460.0
25^{o}C	987.3	658	254.5	588.7
30^{o}C	1240.5	803	356.2	751.5
35^{o}C	1594.9	1047.9	508.9	941.0
ΔH (KJ/mol)	25.23	26.16	53.76	27.6
ΔS (KJ/K^{-1}mol^{-1})	0.07	0.075	0.154	0.08
γ (T = 15-35^{o}C)	1.35-1.44	1.04-1.09	3.57-7.60	1.14-1.24
a	-0.002	-0.0008	-0.0398	-0.0045
b	0.3897	0.077	2.6482	0.2837

The measured solubility and calculated activity coefficients determined in this study were found to be consistent with literature data [26, 81, 82] (see Figure 7). The solubility of ibuprofen is relatively high in ethanol, ethyl acetate and toluene and much lower in acetonitrile which can be rationalized by the polarity that 'like dissolves like'. A non-polar compound will be most likely to be dissolved by non-polar solvents and vice versa. The solvent polarity can be assessed through its dipole moment. Ibuprofen is an organic compound with medium polarity due to containing both polar (-COOH group) and non-polar (benzene ring and substituted group $-C_2H_6$ attached to benzene ring) functional groups. While the dipole moment of ethanol, ethyl acetate and toluene is lower than that of acetonitrile (shown in Table 1), ibuprofen has a high solubility in ethanol, ethyl acetate and toluene but a much lower solubility in acetonitrile. Consequently, the activity coefficient of ibuprofen in acetonitrile (3.57 -7.69) is higher than that in ethanol, ethyl acetate and toluene (1.04 – 1.35). In acetonitrile, where γ values are much greater than 1.0, the solution behavior becomes closer to ideality as the temperature increases. The high values of γ in acetonitrile reflect the stronger solute-solute interactions and concomitantly weaker interactions between the ibuprofen and acetonitrile molecules. In contrast, the almost ideal values of γ in ethyl acetate, ethanol and toluene are consistent with much stronger solute/solvent interactions reflecting the more equality of interaction strengths between constituent molecules in solution i.e. less dependence on to whether solute or solvent.

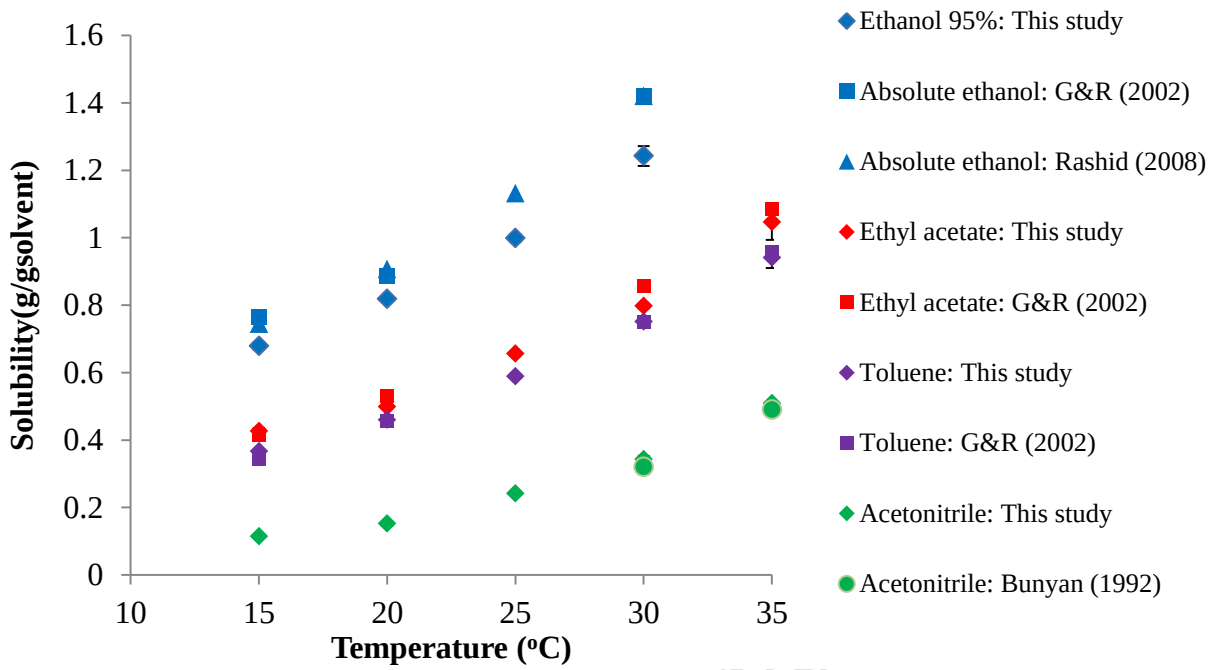

Figure 7 Comparison of the measured solubility in this study and from literature

4.2 Growth rates of {001} and {011} as a function of growth environment

A full set of the experimental growth rate data provided in this paper is given in the section S2 of the supplementary materials.

The data comprises a total of 125 single ibuprofen crystals, spontaneously nucleated in 120-130 growth runs measured in 95% ethanol/water, ethyl acetate, acetonitrile and toluene over a supersaturation range from 0.54 to 1.31 at 2 scale sizes 0.5 and 15 mL.

A sequence of images of crystals grown in various solvents in the in-situ 0.5mL crystallization cell is shown in Figure 8. An example of the plot the distance from the center of the crystals along the growth normal as measured for 5 crystals in the 15ml growth cell to the faces as a function of time (Figure 9) together with the ATR UV/Vis spectra of ibuprofen in 95% ethanol/water during crystallization in the 15mL jacketed vessel is given in Figure 10 and the mean growth rates for the {001} and {011} faces are summarised in Table 2.

(a) (b)

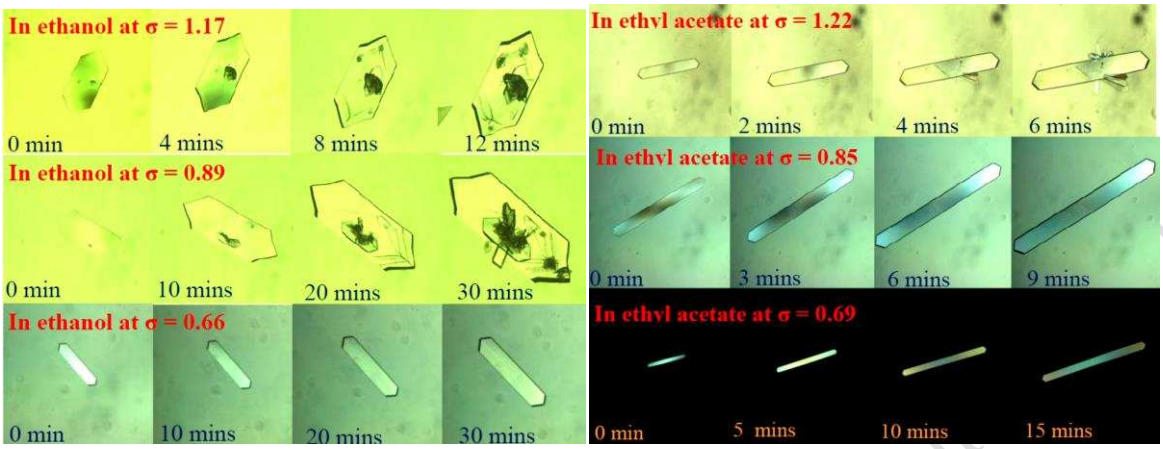

(c) (d)

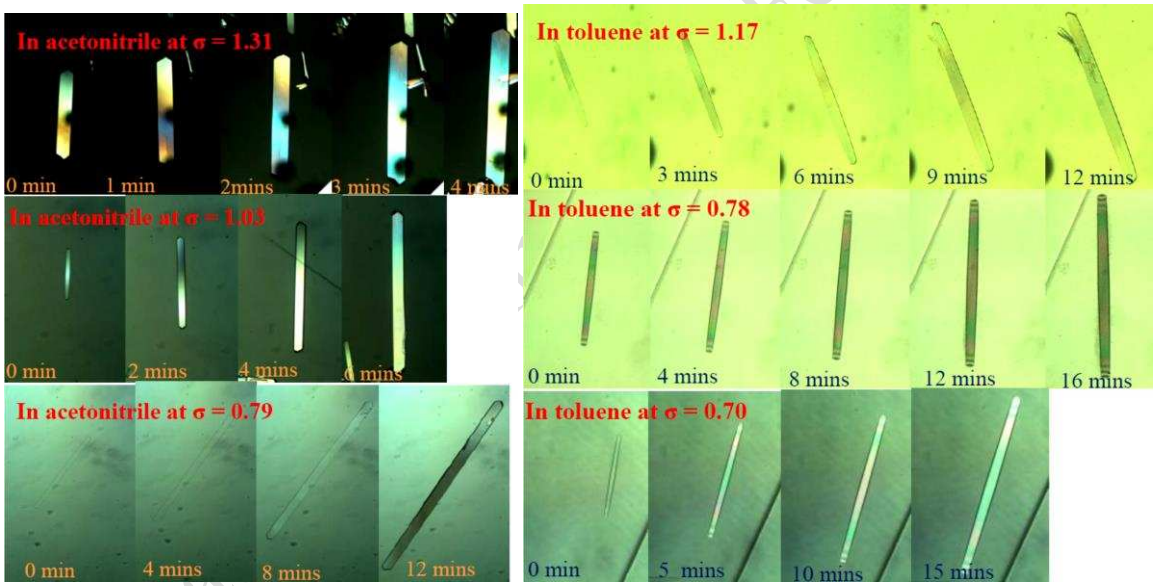

Figure 8 Series of optical micrographs of ibuprofen crystals grown in ethanol 95% between σ = 1.17 and σ = 0.66 (a), in ethyl acetate between σ = 1.20 and σ = 0.69 (b), in acetonitrile between σ = 1.12 and σ = 0.79 (c) and in toluene between σ = 1.17 and σ = 0.70 (d) at the 0.5ml scale size showing the growth of the crystals and their morphology as a function of solvent, elapsed time and solvent supersaturation.

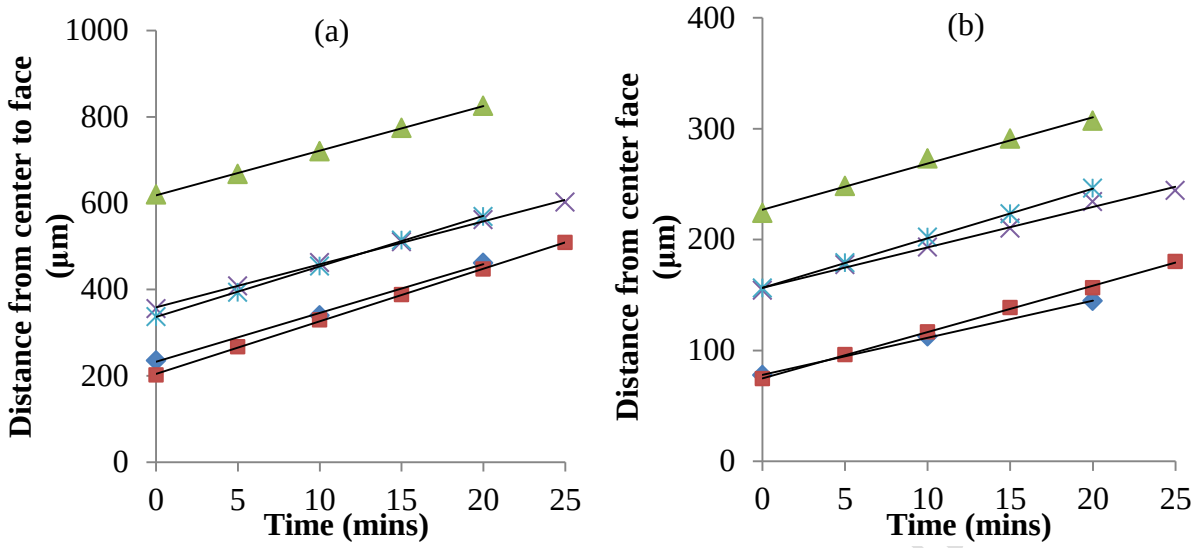

Figure 9 An example of plot of the distance from the center of the crystals along the growth as measured for 5 crystals in the 15ml growth cell to the faces as a function of time. The slope of the line gives the measured growth rate of the face for the estimation of the growth rate for the {011} and {001} face. Each line presents for the growth rate of individual crystals over time: (a) the {011} face in ethanol at σ = 0.66 and (b) the {001} face in ethanol at σ = 0.66

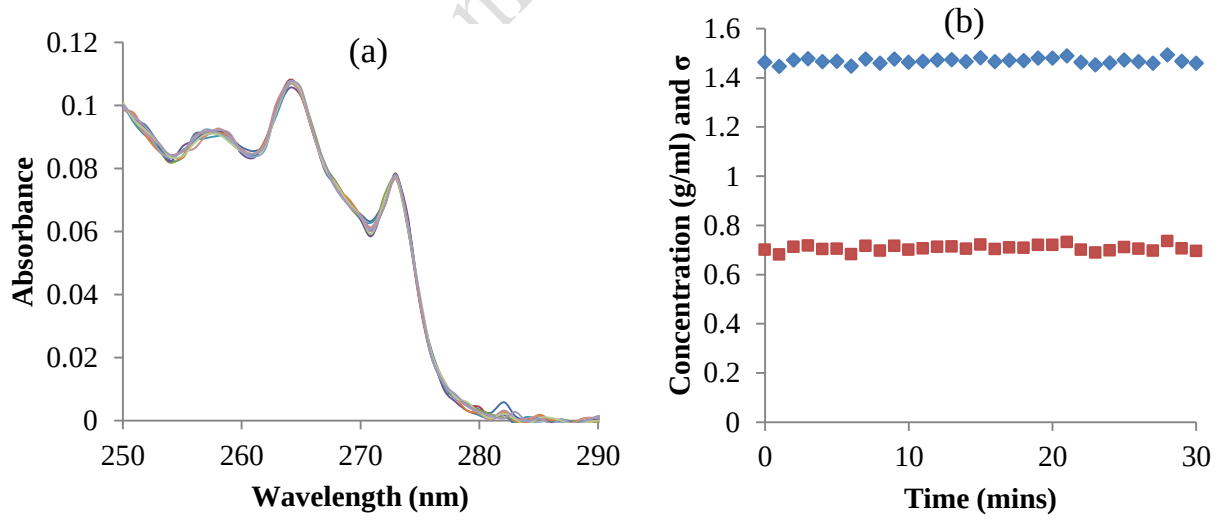

Figure 10 An example of ATR UV/Vis spectra of ibuprofen in ethanol 95% during crystallization in the 15mL jacketed vessel as obtained every minute over the period of 30 mins (a); Solute concentration (blue) and relative supersaturation (red) calculated from the UV-Vis absorbance calibration model (b)

Table 2 Mean growth rates of {011} and {001} faces of ibuprofen in ethanol 95%, ethyl acetate and acetonitrile and toluene in the 0.5ml cell and jacketed-vessel 15ml

Choice of solvents	S-1(σ)	Number of crystals	Mean Growth Rate R(μm/min)			
			$R_{\{001\}}$		$R_{\{011\}}$	
			0.5ml scale	15ml scale	0.5ml scale	15ml scale
Ethanol 95%	0.66	5	3.6 ± 0.7	3.8 ± 0.5	8.5 ± 2.1	11.1 ± 0.8
	0.79	8	4.6 ± 0.4	5.6 ± 1.0	11.8 ± 1.1	14.9 ± 1.4
	0.89	5	6.2 ± 0.8	7.2 ± 0.8	14.3 ± 1.5	16.9 ± 0.9
	0.97	5	8.0 ± 0.9	8.9 ± 0.4	16.6 ± 1.7	18.4 ± 1.1
	1.17	5	13.2 ± 1.6	13.2 ± 0.7	21.6 ± 1.3	24.6 ± 4.1
Ethyl acetate	0.54	6	1.8 ± 0.3	1.9 ± 0.3	17.7 ± 2.0	19.1 ± 3.7
	0.69	5	3.4 ± 0.4	3.9 ± 0.9	31.6 ± 1.8	36.5 ± 3.0
	0.76	6	4.4 ± 0.6	5.8 ± 0.4	37.5 ± 3.1	41.7 ± 4.1
	0.85	7	6.3 ± 0.4	6.6 ± 0.7	42.5 ± 3.2	47.1 ± 2.1
	0.97	7	8.3 ± 0.8	10.1 ± 0.8	48.9 ± 3.7	53.0 ± 2.2
	1.06	7	9.7 ± 0.8	12.6 ± 0.5	52.1 ± 6.6	58.6 ± 3.3
	1.20	7	12.2 ± 2.6	13.8 ± 1.2	61.3 ± 7.7	65.4 ± 3.7
Acetonitrile	0.79	6	3.6 ± 0.7	4.8 ± 1.0	51.5 ± 5.2	56.3 ± 5.0
	0.93	5	5.0 ± 0.3	5.8 ± 0.3	60.0 ± 6.7	72.9 ± 3.5
	1.03	6	7.4 ± 2.0	9.3 ± 0.6	79.9 ±11.5	85.4 ± 7.9
	1.12	6	10.7 ± 2.0	12.7 ± 1.4	90.0 ± 11.7	104.9 ± 8.8
	1.31	6	14.6 ± 2.6	16.9 ± 1.4	112 ± 12.5	121.4 ± 12.6
Toluene	0.7	6	1.8 ± 0.2	2.4 ± 0.5	27.8 ± 1.8	32.0 ± 2.3
	0.78	5	2.1 ± 0.2	2.8 ± 0.5	30.5 ± 2.6	33.6 ± 4.4
	0.86	6	3.2 ± 0.6	3.5 ± 0.8	34.1 ± 4.2	38.7 ± 3.1
	1.17	6	4.4 ± 1.7	5.0 ± 0.4	40.2 ± 5.1	43.8 ± 2.4

The growth rate of the {011} and {001} faces of ibuprofen in ethanol in this study was compared to previous kinetic studies on organic materials (Table 3) and also to previous work on ibuprofen by Rashid et al [11] (Table 4). In the latter case the kinetic data was modelled using an empirical rate equation:

$$G = k_G \sigma^n \quad (19)$$

where G is the linear growth rate which is calculated by dL/dt (L is a characteristic crystal size taken as the volume median size of the distribution), k_G is the growth rate coefficient and n is the kinetics order.

In this the fitting revealed that k_G = 15 and n = 1.

Table 3 Comparison of the mean growth rates with the growth rate calculated from Rashid [11]

Supersaturation σ	**This study**		**Data after Rashid** [11]
	Face {001}	**Face {011}**	
0.66	3.6 - 3.8	8.5 - 11.1	9.9
0.79	4.6 – 5.6	11.8-11.9	11.85
0.89	6.2 – 7.2	14.3 – 16.9	13.35
0.97	8.9 - 8.9	16.6 - 18.4	14.55
1.17	13.2	21.6 - 24.6	17.55

Table 4 The growth rate of some organic materials from literature

Compounds	T (^oC)	σ	Mean growth rate (μm/min)	References
Tripalmitin (melt)	47 – 52		12 – 27	Staple, A.G. F et al. [12]
Paracetamol in 60% methanol and 40% water		0.25	18	O'Ciardha et al.[48]
L-Glutamic Acid		0.47- 0.5	R_L: 1.5 – 1.9 R_W: 0.3 – 0.36	Wang, X. Z. et al. [13]
Paracetamolin the [110], [010] and [001] direction		0.06 -0.26	1.2 – 9.6	Finnie, S. D. et al. [83]

* $R_L$and R_W : Growth rate for length and width of needle-like crystals

The mean growth rates (R) of the {001} and {011} faces increase quite significantly with increasing relative supersaturation. R{001} and R{011} are responsible for defining the in-plane shape of the crystals. For all the solvents studied, R{011} was found to be greater than R{001}, in particular for crystals grown in ethyl acetate, acetonitrile and toluene. This anisotropy results in crystal morphologies with higher aspect ratios notably more elongated crystals in ethyl acetate,

acetonitrile and toluene solutions (see Figure 12). No significant differences were observed between the two scale sizes. Considering the four solvents together, for solutions at the same supersaturation level, R{011} in acetonitrile was found to be the highest and R{011} in ethanol the lowest. R{001} of ibuprofen crystals in ethanol and ethyl acetate were found to be fairly similar and R{001} in acetonitrile lower. R{011} in acetonitrile was found to increase much more with increasing supersaturation when compared to other solvents. The rate of change of growth rate with changing supersaturation ($dR/d\sigma$) for the {001} and {011} faces in the four solvents was not found to follow a linear relationship. Specifically, in ethyl acetate the gradients of R{011} with supersaturation ($d_{R\{011\}}/d\sigma$) for $\sigma > 0.76$ were found to be lower than those measured for $\sigma \leq 0.76$. At $\sigma < 0.76$ $d_{R\{011\}}/d\sigma$ is 90.4 and $d_{R\{001\}}/d\sigma$ is 11.6 but at $\sigma > 0.76$ $d_{R\{011\}}/d\sigma$ is 50.7 and $d_{R\{001\}}/d\sigma$ is 17.4.

At the 15ml scale, R{001} and R{011} were found to be greater than that found for the measurements at 0.5ml. According to Noyes and Whitney [84], the driving force for crystal growth is the difference between the concentration in the bulk of solution and at the solid surface. As crystals start to grow, the concentration drops at the interface between the boundary layer of solution adjacent to it thus facilitating the concentration gradient with respect to the bulk solution which drives the solute diffusion process through which solute molecules move from the bulk solution phase to the growing crystal. It can be postulated that the mass transfer for the larger scale size, due to the larger solution volume consistent with a faster diffusion rate would be greater at the 15ml solution when compared to the 0.5ml scale size. Hence it can be expected that the driving force for the crystal growth should be somewhat less in the 0.5mL cuvette. With the same amount of crystals forming for both scale sizes, the local supersaturation levels might be expected to decrease faster in the smaller 0.5mL solution when compared to that in the 15mL

cell. However, examination of the ATR UV/Vis data measured in-situ in the 15mL cell shows supersaturation level to be comparatively constant during the crystallisation process. This probably reflects the small amount of crystals nucleated in the vessel resulting in only a modest and perhaps un-detectable supersaturation change.

4.3 Crystal morphology as a function of growth environment

The morphology of ibuprofen crystals as a function of solvent and supersaturation was found to be quite consistent from crystal to crystal and between two scale sizes in good agreement with previous studies [2, 26, 27]. Plate-like 'hexagonal' crystals were obtained from ethanol whilst more elongated forms were found in ethyl acetate, acetonitrile and toluene. Crystals prepared from toluene and acetonitrile solutions were found to grow with the most needle-like morphology. The former exhibited a degree of curvature on the {001} faces which might be consistent with the onset of kinetics roughening. The microscopic images obtained were of very high quality revealing the traces of the growth sector boundaries and revealing no evidence for the presence of a substantial level of crystal defects such as solvent inclusions, twining etc. Changes of relative growth rate of the {001} and {011} faces with solvent-type and supersaturation resulted in a variation of the crystal aspect ratios reflecting the fact that the crystals tended to be more elongated in the polar aprotic and non-polar solvents and with decreasing supersaturation, as shown in Figure 11 and Figure 12. Similar effects were reported by Ristic, et al. [85] who observed that the growth morphology of monoclinic paracetamol from pure aqueous solution at different supersaturations exhibited a strong supersaturation-dependence associated with a change from a columnar to a plate-like habit with increasing supersaturation.

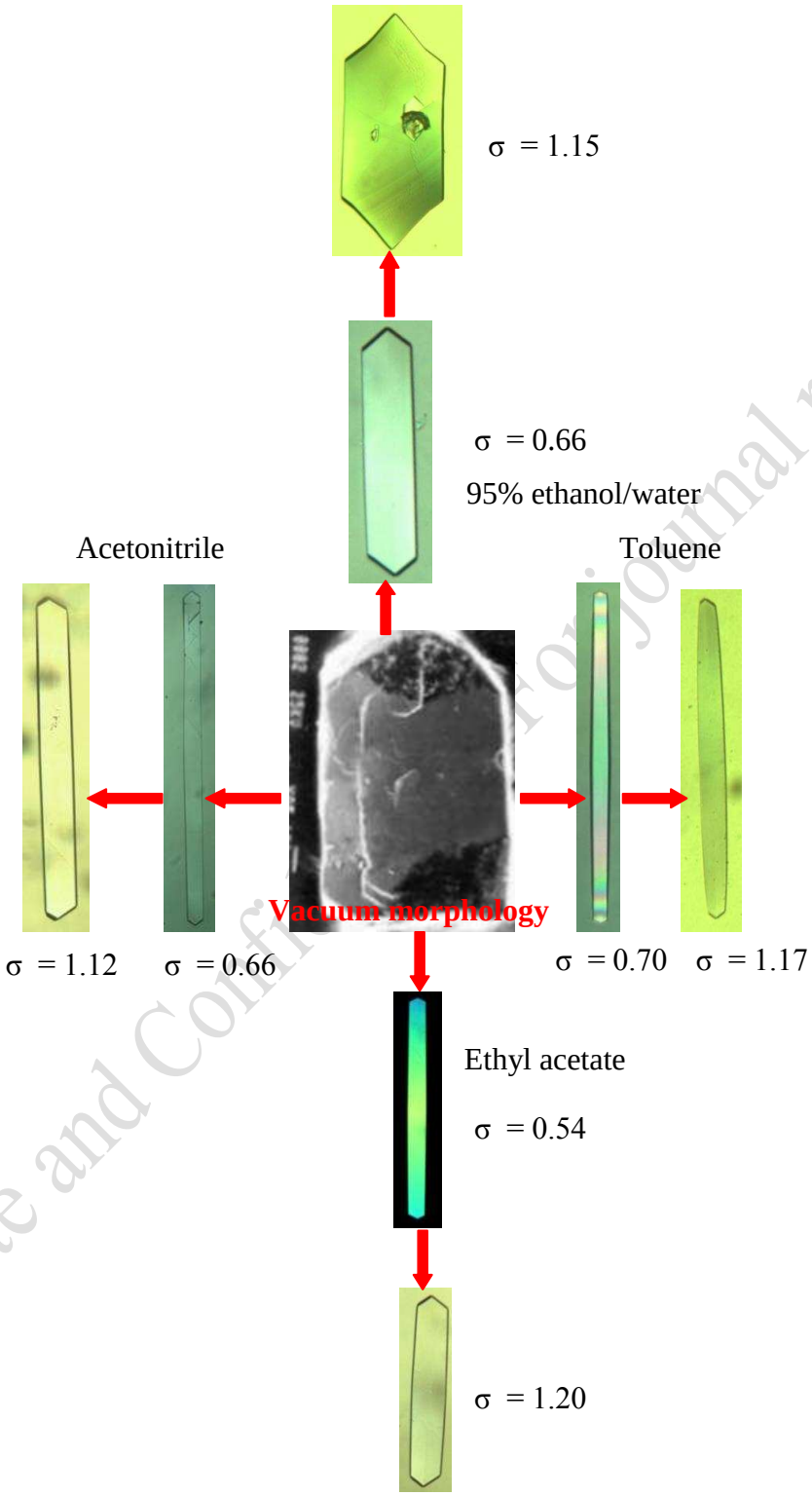

Figure 11 Representative micrographs taken from in-situ images at 0.5mL scale size summarizing the influence of solvent and supersaturation on the growth morphologies of ibuprofen together with the

vacuum morphology figure from Bunyan [26]. Note that the aspect ratios mostly tend to increase with decreasing supersaturation.

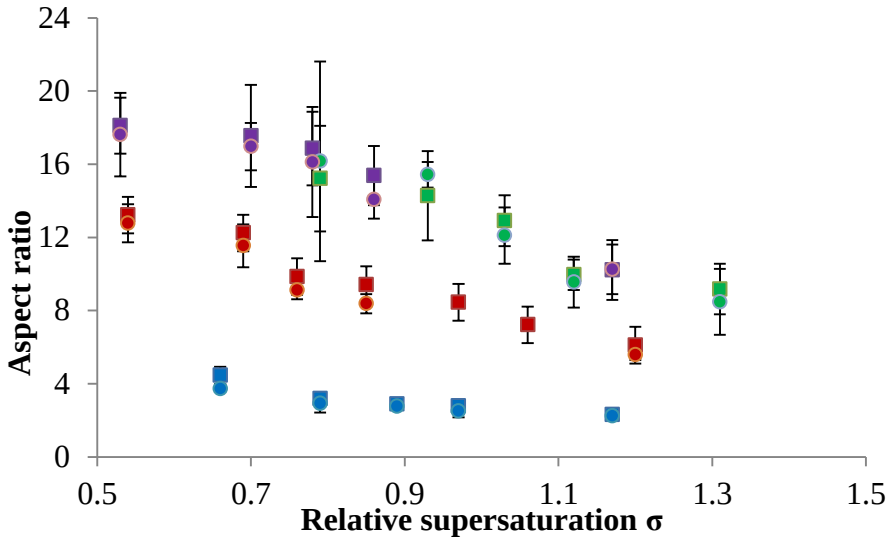

Figure 12 Aspect ratios of ibuprofen crystal grown from 95% ethanol/water (blue), ethyl acetate (red), acetonitrile (green) and toluene (purple) versus relative supersaturation at two scale-sizes: 0.5ml (squares) and 15ml (circles).

It was found that at higher levels of supersaturation for all solvents (particularly ethanol) the crystals were found to present significantly large higher order re-entrant faces at the boundary between {011} and {01-1}, see Figure 13. The mechanistic origin of this effect is currently being characterised in further detail and the results will be presented in a future publication.

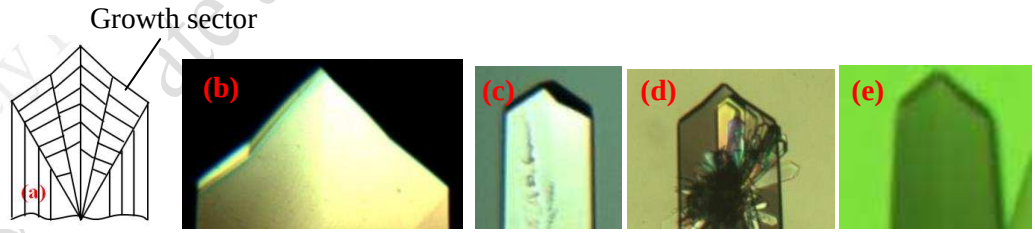

Figure 13 Schematic (a) and pictures of ibuprofen crystal grown from 95% ethanol/water (b), acetonitrile (c), ethyl acetate (d), and toluene (e) showing the emergence of higher index re-entrant faces at the boundary between the end-capping {011} faces

The morphology of a crystal in different growth environments depends, collectively, on the relative growth rates associated with its constituent crystal habit faces. Mechanistically, these rates reflect the balance between the rate of desolvation of solvent molecules and the rate of solute adsorption at the different crystal growth interfaces. Ultimately these rates are linked to the respective interaction energies associated with the solute and solvents molecules on these surfaces. Hence, the growth rate of an individual habit face can be rationalised in terms of the respective binding between solute and solvents on specific faces using molecular modeling to examine the molecular arrangements present on at the {011} and {001} surfaces as shown in Figure 14.

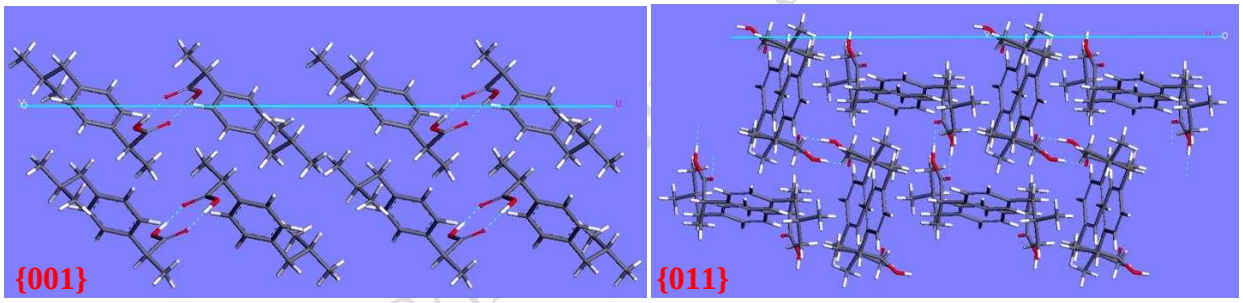

Figure 14 Molecular packing diagrams based upon the crystallographic structures: (left) the {001} face showing its hydrophobic nature with -CH_3 groups exposed at the surface with the protic COOH groups exposed in one direction and in a quite restricted position; (right) {011} face showing a more polar surface with exposed–COOH groups at the surface with two different directions that are more exposed and easier accessible than –COOH group on face {001} which provides good binding sites for polar solvent molecules.

On the {011} face the molecules can be seen to be arranged alternatively nearly parallel and perpendicular to the surface and exhibits great hydrophilicity because the -COOH groups are more exposed and easier accessible for the formation of the hydrogen bonds hence so the use of polar

protic solvents (ethanol with -OH groups which can act either as a hydrogen bond donors or acceptors) would inhibit the growth of {011} resulting in shortened crystals (plate-like crystals). On the contrary, the more polar aprotic (ethyl acetate or acetonitrile) or non-polar (toluene) solvents would be less likely to interact on the {011} surface and more likely to bind to the hydrophobic {001} surfaces thus resulting more elongated crystals for theses solvents. Moreover, interactions of less polar solvents with alkyl groups on the {001} face hinders the growth of this face.

4.4 Variation in growth rates between crystals prepared under the same conditions

Each crystal growth rate data point reported in Table 2 represents a mean value from between five and eight individual crystals for which the growth rate was measured. Figure 9 illustrates the growth of the {001} and {011} face over time for five individual crystals. The face specific growth rates were found to display a good linear fit with time for each crystal surface indicating that these surfaces follow the constant crystal growth model which proposes a constant relative growth rate of each crystal during the growth period, albeit with different growth rates for different crystals. The average standard deviation of these particular crystal measurements was found to be about 12%. The % crystal growth rate variation crystal by crystal and for both faces was found to increase with an increase in the mean growth rate in a similar manner to previous observations made on citric acid monohydrate [86], sucrose [87], and proteins [18]. The growth rate variations of ibuprofen are summarised in Table 5. Comparing these data with that from other organic and inorganic materials (see Table 6) shows a good broad agreement.

Table 5. The coefficient of variation (%) for the growth rate of the crystal faces

Solvent type	The {001} face		The {011} face	
	0.5mL	15mL	0.5mL	15mL
Ethanol	0.12	0.103	0.12	0.09
Ethyl acetate	0.123	0.10	0.095	0.07
Acetonitrile	0.177	0.103	0.12	0.083
Toluene	0.193	0.173	0.092	0.084

Table 6. Growth Rate Dispersion of some other organic and inorganic materials

Materials	The coefficient of variation	References
Lysozyme (face {110})	0.05 - 0.2	Judge et al. [18]
Lysozyme (face {101})	0.05 - 0.33	Judge et al. [18]
Paracetamol (face {110})	0.061 - 0.141	Finnie et al. [83]
Sucrose	0.28	Berglund and Murphy [87]
Citric acid monohydrate	0.35	Berglund and Larson [86]
ADP	0.37	Garside and Ristic [17]
Ibuprofen	0.07- 0.19	This study

However, caution should be exercised in over interpreting this data as errors e.g. due to the blurring of the crystal boundaries together with minor errors from manual measurements etc. could have been introduced. Nonetheless, the standard deviations of the measured growth rates are broadly representative of the expected variation in growth rates of crystal habit faces in individual crystals. According to observations of sequence of single crystals grown during a period of time, there were different growth rate between four similar faces (011), (0-11), (01-1) and (0-1-1) faces and each crystal grows at slightly different rate in the same conditions. Given

that the initial size of crystals studied was very similar, these observations are more consistent with being due to growth rate dispersion (GRD) rather than one of size dependant growth (SDG).

In this study, the growth rate data shows a lower growth rate variation for the growth of spontaneously nucleated crystals in stagnant, supersaturated solutions compared to the GRD observed in a stirred batch crystallizer which was measured from size distribution of crystals from seeding [11]. The latter study showed ibuprofen growth in absolute ethanol at the 1L stirred seeded batch crystallisation vessel size exhibits GRD with a log normal distribution of growth rates having a spread of the coefficient of variation CVv = 0.5 (Figure 15). Similarity, studies of the growth rate behaviour of anhydrous sodium sulphate revealed that GRD of single crystals grown in a flow cell was less than that found among a population of crystals prepared in a batch crystallizer [88]. This latter data was rationalised in terms of the crystal collisions occurring in the agitated crystalliser producing greater numbers of faster growing nuclei.

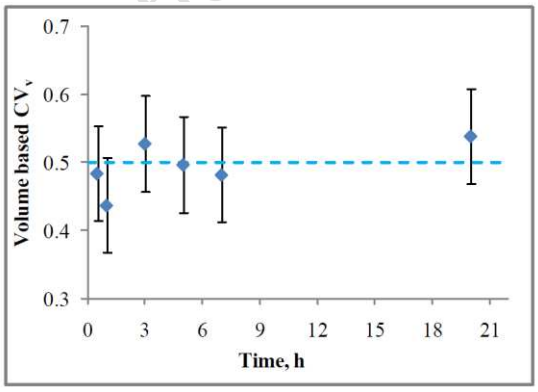

Figure 15 Distribution spread CV_v versus experimental growth time at 25°C in absolute ethanol (reproduced with permission from Rashid et al.[11])

Whilst a significant number of studies have been carried out, the mechanism of GRD is still a matter of some debate. The growth rate of the {001} and {011} faces showed a trend of higher

GRD at the higher supersaturations and the GRD in the 15 mL vessel is less than that observed for the 0.5 mL cuvette. These observations are similar to the data recorded for other materials citric acid monohydrate [86], sucrose [87], and proteins [18]. At the higher supersaturations, the nucleation rate was found to be greater, which means more crystals are generated in the in-situ cell which grow at the same time in solution resulting in a more rapid desupersaturation of the growth solution at the smaller scale size (0.5 mL). The GRD effect was not found to vary significantly between the solvents except for toluene. However, this observation might due to the very needle-like crystals produced with this solvent, e.g. curvy {001} faces which were found in toluene.

4.5 Characterisation of the interfacial growth mechanisms

The microscopy observations reveal that the crystal growth was clearly planar in nature. This, together with the appearance of crystals which are bounded by well-defined crystallographic surfaces which are not roughened would suggest that the growth mechanism would be either due to the BCF or B&S mechanism. This supposition is confirmed through examination of data presented in Figure 16 which show that there is a strong and non linear dependence of the relative growth rates, on supersaturation ruling out models, such as the rough surface model [71] for which a linear dependence of growth rate on supersaturation fitting would be expected. Plots of the measured crystal growth rates versus relative supersaturation together with fitting against both these models are given in Figure 16.

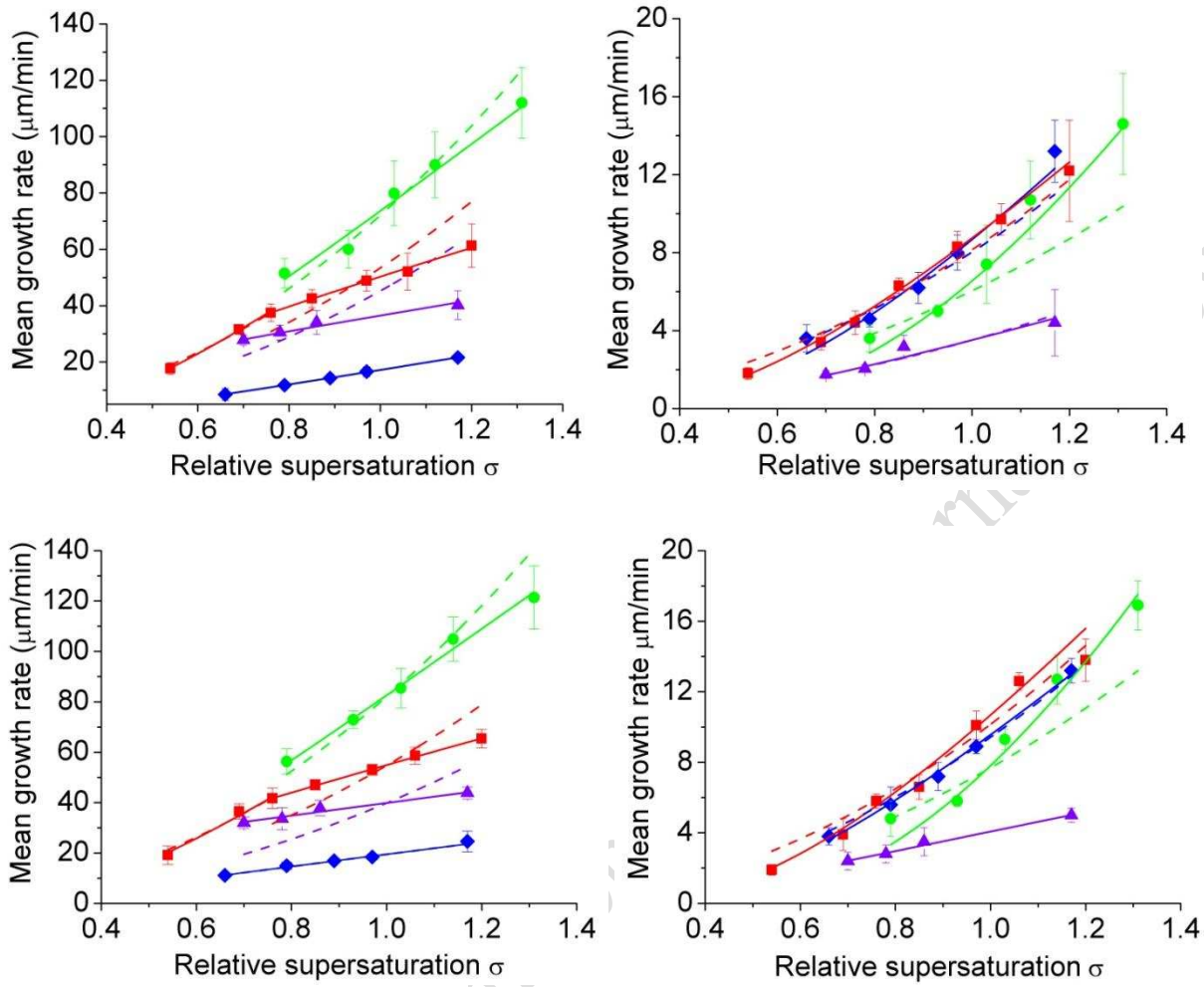

Figure 16 Plots of the growth rate versus relative supersaturation in ethanol (blue), ethyl acetate (red), acetonitrile (green) and toluene (purple) together with fitted B&S (solid lines) and BCF (dotted lines) mechanism models for both {011} (left) and {001} (right) and for both 0.5mL (top) and 15mL (bottom)

Table 7 Fitting parameters for the faces {011} and (002) of ibuprofen grown in ethanol 95%, ethyl acetate, acetonitrile and toluene with BCF model (equation 10) and B&S model (equation 11) together with the adj.R^2

Solvent choice		0.5 mL				15 mL			
		{011} face		{001} face		{011}face		{001}face	
		B&S	BCF	B&S	BCF	B&S	BCF	B&S	BCF
Ethanol 95%	A	41.782	16.540	39.41	8.03	29.13	33.97	32.28	9.42
	B	-0.962	8.79E8	-1.51	4.2E11	-0.40	0.65	-1.22	3.30E8
	adj.R^2	0.986	0.966	0.94	0.94	0.99	0.99	0.996	0.992

Ethyl acetate (σ = 0.54-0.76)	A B adj.R^2	152.62 -0.88 0.996	65.02 63.46 0.973	31.94 -1.29 0.994	8.15 2.2E9 0.95	162.55 -0.85 0.97	72.95 61.89 0.95	41.57 -1.36 0.986	10.16 8.3E12 0.941
Ethyl acetate (σ = 0.76-1.20)	A B adj.R^2	61.53 -0.20 0.995	53.41 49.22 -0.22			63.56 -0.15 0.998	54.75 48.74 -0.28		
Acetonitrile	A B adj.R^2	167.66 -0.81 0.937	72.09 37.45 0.872	70.88 -2.38 0.891	6.05 2.0E8 0.70	175.15 -0.75 0.99	82.03 32.75 0.88	91.95 -2.47 0.932	7.69 1.91E6 0707
Toluene	A B adj.R^2	33.76 0.078 0.958	45.25 24.89 -5.77	9.56 -1.00 0.77	3.51 46.2 0.76	32.46 0.21 0.97	39.82 8.07 -5.86	6.902 -0.528 0.994	5.858 0.857 0.994

Table 7 showed shows the fitting parameters A and B (see equation (10) and (11)) and the adj. R^2 for the faces {011} and {001} grown in various solvents fitted against the B&S and BCF models. Generally and overall, the B&S model provides a better fit to the data than that for BCF model for most data measured. The main exceptions are for R{011} and R{001} in ethanolic solutions, which provided broadly similar values for the fitting adj. R^2 (0.97-0.99) for both models.

In ethyl acetate, the growth rate was studied at lower range of supersaturations, i.e. from 0.54 to 1.2. It was shown that at supersaturation σ from 0.54 to 0.76 R{011} versus σ fits well for both BCF and B&S model (the adj. R^2 = 0.996 and 0.973, respectively). However, at σ ranging 0.76 to 1.20 only the B&S shows acceptable fit (the adj. R^2 = 0.995 for B&S and -0.22 for BCF) consistent with the growth mechanisms where the BCF mechanism might be occur at low supersaturation [71]. At intermediate supersaturations (σ from 0.54 to 0.76) spiral growth and birth and spread mechanisms may both be present. However, at higher supersaturation (σ from 0.76 to 1.20) the B&S mechanism provided a better fit to the data. This observation might suggest a change of the growth mechanism between these two supersaturation regions.

In summary, the crystals grown from four solvents were mostly found to be consistent with crystal growth mediated by the B&S mechanism over the range of supersaturations from 0.54 to

1.31. For some solvents and supersaturations the BCF model was also found to provide an acceptable fit. In addition the data revealed no significant evidence for any mechanistic changes associated with crystal growth between scale sizes.

5 Conclusions

The solution mediated crystal growth rates of the {011} and {001} faces of spontaneously nucleated ibuprofen crystals have been measured as a function of supersaturation and solvent under diffusion-limited conditions at two scale sizes (0.5mL and 15mL). The results show that the mean growth rate of the {001} and {011} faces were found to increase with increasing relative supersaturation with $R_{\{011\}}$ being higher than $R_{\{001\}}$. This is found particularly to be the case for crystals grown in ethyl acetate, acetonitrile and toluene solutions at the two different scale sizes.

At a similar supersaturation level, $R_{\{011\}}$ were found to be lowest in ethanol and highest in acetonitrile with $R_{\{001\}}$ lowest in toluene and highest in ethanol and ethyl acetate. The difference in the growth rates between different crystal surfaces as well as the growth rate of the same surface when grown from different solvents can be rationalised in terms of the differences in the inter-molecular interactions between crystal surfaces and the solvents. Changes in the relative growth rate of the {001} and {011} faces with solvent type and supersaturation level cause a change in the crystal aspect ratios associated with the crystals becoming more elongated in ethyl acetate, acetonitrile and toluene solutions in comparison to the crystals grown in 95% ethanol/water. The aspect ratios for crystals grown at 0.5 mL and 15 mL scale-sizes were found to be quite similar. GRD was found to occur for crystal growth on both surfaces and at all supersaturation levels. However, it was found to be less pronounced when compared to the case of crystals prepared in a stirred batch crystallizer (Rashid et al., 2012). The growth rates $R_{\{001\}}$

and $R_{\{011\}}$ in the 15 mL vessel are greater than the growth rates in the 0.5 mL cuvette possibly due to better mass transfer environment in the larger vessel and due to the fact that supersaturation levels probably decrease more rapidly in the smaller vessel. However, the GRD measured in the 15 mL vessel was found to be less than the GRD in the 0.5 mL cuvette. The supersaturation σ at the 15 mL scale as measured in-situ using an ATR UV/Vis spectrophotometer was found to be nearly constant during the growth process, supporting the utility of this methodology for the routine determination of the growth kinetics and mechanism. The B&S interfacial kinetic model was found to describe best the dependence of the growth rate of the {011} face and {001} face on the supersaturation σ from 0.54 to 1.22, albeit for a few cases the BCF mechanism was also found to fit that data satisfactorily.

Acknowledgement. The authors gratefully acknowledge the financial support of this work by Pfizer and UK Northern Universities (N8) METRC initiative in molecular engineering. We also thank Prof. Ted White (University of Queensland, Australia) for his most helpful comments and discussions concerning the growth rate measurements of ibuprofen.

We also gratefully acknowledge the UK's EPSRC for their support in nucleation research at the Universities of Leeds and Manchester through their funding of the Critical Mass Project "Molecules, Clusters and Crystals" (grant references EP/I014446/1 and EP/I013563/1, respectively).

References

1. Beckmann, W., Simultaneous measurement of the growth rates of the (001) and (110) faces of stearic acid growing from solution. Journal of Physics E: Scientific Instruments, 1986. **19**(6): p. 444.
2. Cano, H., N. Gabas, and J. Canselier, Experimental study on the ibuprofen crystal growth morphology in solution. Journal of Crystal Growth, 2001. **224**(3): p. 335-341.
3. Davey, R., W. Fila, and J. Garside, The influence of biuret on the growth kinetics of urea crystals from aqueous solutions. Journal of Crystal Growth, 1986. **79**(1): p. 607-613.
4. Davey, R. and J. Mullin, Growth of the {100} faces of ammonium dihydrogen phosphate crystals in the presence of ionic species. Journal of Crystal Growth, 1974. **26**(1): p. 45-51.
5. Davey, R. and J. Mullin, Growth of the {101} faces of ammonium dihydrogen phosphate crystals in the presence of ionic species. Journal of Crystal Growth, 1974. **23**(2): p. 89-94.
6. Sweegers, C., H. Meekes, W. Van Enckevort, I. Hiralal, and A. Rijkeboer, Growth rate analysis of gibbsite single crystals growing from aqueous sodium aluminate solutions. Crystal Growth & Design, 2004. **4**(1): p. 185-198.
7. Arellano, M.a.P., J.M. Aguilera, and P. Bouchon, Development of a digital video-microscopy technique to study lactose crystallisation kinetics in situ. Carbohydrate Research, 2004. **339**(16): p. 2721-2730.
8. De Anda, J.C., X. Wang, X. Lai, K. Roberts, K. Jennings, M. Wilkinson, D. Watson, and D. Roberts, Real time product morphology monitoring in crystallization using imaging technique. AIChE journal, 2005. **51**(5): p. 1406-1414.
9. Li, R., G. Thomson, G. White, X. Wang, J.C. De Anda, and K. Roberts, Integration of crystal morphology modeling and on‐line shape measurement. AIChE journal, 2006. **52**(6): p. 2297-2305.
10. Ma, C.Y., X.Z. Wang, and K.J. Roberts, Multi-dimensional population balance modeling of the growth of rod-like L-glutamic acid crystals using growth rates estimated from in-process imaging. Advanced Powder Technology, 2007. **18**(6): p. 707-724.
11. Rashid, A., E. White, T. Howes, J. Litster, and I. Marziano, Growth rates of ibuprofen crystals grown from ethanol and aqueous ethanol. Chemical Engineering Research and Design, 2012. **90**(1): p. 158-161.
12. Stapley, A.G., C. Himawan, W. MacNaughtan, and T.J. Foster, A computational method for extracting crystallization growth and nucleation rate data from hot stage microscope images. Crystal Growth & Design, 2009. **9**(12): p. 5061-5068.
13. Wang, X., J. Calderon De Anda, and K. Roberts, Real-time measurement of the growth rates of individual crystal facets using imaging and image analysis: a feasibility study on needle-shaped crystals of L-glutamic acid. Chemical Engineering Research and Design, 2007. **85**(7): p. 921-927.
14. Wang, X., J. Calderon De Anda, K. Roberts, R. Li, G. Thomson, and G. White, Advances in on-line monitoring and control of the morphological and polymorphic forms of organic crystals grown from solution. KONA (Powder and Particle), 2005. **23**: p. 69-85.
15. Ristić, R., J. Sherwood, and K. Wojciechowski, Assessment of the strain in small sodium chlorate crystals and its relation to growth rate dispersion. Journal of Crystal Growth, 1988. **91**(1): p. 163-168.

16. Davey, R., R. Ristić, and B. Žižić, The role of dislocations in the growth of ammonium dihydrogen phosphate crystals from aqueous solutions. Journal of Crystal Growth, 1979. **47**(1): p. 1-4.
17. Garside, J. and R. Ristić, Growth rate dispersion among ADP crystals formed by primary nucleation. Journal of Crystal Growth, 1983. **61**(2): p. 215-220.
18. Judge, R.A., E.L. Forsythe, and M.L. Pusey, Growth rate dispersion in protein crystal growth. Crystal Growth & Design, 2010. **10**(7): p. 3164-3168.
19. Derdour, L., C. Sivakumar, D. Skliar, S. Pack, C. Lai, J. Vernille, and S. Kiang, Crystallization from Solutions Containing Multiple Conformers. 2. Experimental Study and Model Validation. Crystal Growth & Design, 2012. **12**(11): p. 5188-5196.
20. Markande, A., A. Nezzal, J. Fitzpatrick, and L. Aerts, Investigation of the crystallization kinetics of dextrose monohydrate using in situ particle size and supersaturation monitoring. Particulate Science and Technology, 2009. **27**(4): p. 373-388.
21. Schöll, J., C. Lindenberg, L. Vicum, J. Brozio, and M. Mazzotti, Precipitation *of α L*-glutamic acid: determination of growth kinetics. Faraday Discussions, 2007. **136**: p. 247-264.
22. Mullin, J.W., Crystallization2001: Butterworth-Heinemann.
23. Shankland, N., A.J. Florence, P.J. Cox, D.B. Sheen, S.W. Love, N.S. Stewart, and C.C. Wilson, Crystal morphology of ibuprofen predicted from single-crystal pulsed neutron diffraction data. Chemical Communications, 1996(7): p. 855-856.
24. Shankland, N., C. Wilson, A. Florence, and P. Cox, Refinement of ibuprofen at 100K by single-crystal pulsed neutron diffraction. Acta Crystallographica Section C: Crystal Structure Communications, 1997. **53**(7): p. 951-954.
25. Dudognon, E., F. Danède, M. Descamps, and N.T. Correia, Evidence for a new crystalline phase of racemic ibuprofen. Pharmaceutical Research, 2008. **25**(12): p. 2853-2858.
26. Bunyan, J., N. Shankland, and D. Sheen. Solvent effects on the morphology of ibuprofen. in AIChE Symposium Series. 1991.
27. Winn, D. and M.F. Doherty, Modeling crystal shapes of organic materials grown from solution. AIChE journal, 2000. **46**(7): p. 1348-1367.
28. Garekani, H., F. Sadeghi, A. Badiee, S. Mostafa, A.R. Rajabi-Siahboomi, and A. Rajabi-Siahboomi, Crystal habit modifications of ibuprofen and their physicomechanical characteristics. Drug Development and Industrial Pharmacy, 2001. **27**(8): p. 803-809.
29. Gordon, R.E. and S.I. Amin, Crystallization of ibuprofen, 1984, Google Patents.
30. Labhasetwar, V., S. Deshmukh, and A. Dorle, Studies on some crystalline forms of ibuprofen. Drug Development and Industrial Pharmacy, 1993. **19**(6): p. 631-641.
31. Nikolakakis, I., K. Kachrimanis, and S. Malamataris, Relations between crystallisation conditions and micromeritic properties of ibuprofen. International Journal of Pharmaceutics, 2000. **201**(1): p. 79-88.
32. Rasenack, N. and B. Müller, Properties of ibuprofen crystallized under various conditions: A comparative study. Drug Development and Industrial Pharmacy, 2002. **28**(9): p. 1077-1089.
33. Rasenack, N. and B.W. Muller, Crystal habit and tableting behavior. International Journal of Pharmaceutics, 2002. **244**(1-2): p. 45-57.
34. Rasenack, N. and B.W. Müller, Ibuprofen crystals with optimized properties. International Journal of Pharmaceutics, 2002. **245**(1): p. 9-24.

35. Omar, W., S. Al‐Sayed, A. Sultan, and J. Ulrich, Growth rate of single acetaminophen crystals in supersaturated aqueous solution under different operating conditions. Crystal Research and Technology, 2008. **43**(1): p. 22-27.
36. White, E. and P. Wright. Magnitude of size dispersion effects in crystallization. in Chemical Engineering Progress Symposium Series No. 1971.
37. Garside, J., A. Mersmann, and J. Nývlt, Measurement of crystal growth and nucleation rates2002: IChemE.
38. Randolph, A., Theory of particulate processes: analysis and techniques of continuous crystallization1971: Academic press.
39. Calderon De Anda, J., X. Wang, X. Lai, and K. Roberts, Classifying organic crystals via in-process image analysis and the use of monitoring charts to follow polymorphic and morphological changes. Journal of Process Control, 2005. **15**(7): p. 785-797.
40. Calderon De Anda, J., X. Wang, and K. Roberts, Multi-scale segmentation image analysis for the in-process monitoring of particle shape with batch crystallisers. Chemical Engineering Science, 2005. **60**(4): p. 1053-1065.
41. Liu, J.J., C.Y. Ma, Y.D. Hu, and X.Z. Wang, Modelling protein crystallisation using morphological population balance models. Chemical Engineering Research and Design, 2010. **88**(4): p. 437-446.
42. Ma, C.Y. and X.Z. Wang, Model identification of crystal facet growth kinetics in morphological population balance modeling of l-glutamic acid crystallization and experimental validation. Chemical engineering science, 2012. **70**: p. 22-30.
43. Ma, C.Y., X.Z. Wang, and K.J. Roberts, Morphological population balance for modeling crystal growth in face directions. AIChE journal, 2008. **54**(1): p. 209-222.
44. Pencheva, R.Y., Monitoring and Controlling Crystal Size during Industrial Batch Crystallization Processes via the Use of Acoustic Attenuation Spectroscopy Techniques. PhD thesis (University of Leeds), 2007.
45. Kwokal, A., D.e. Ćavužić, and K.J. Roberts, Surface Adsorbed Templates for Directing the Crystal Growth of Entacapone as Monitored Using Process Analytical Techniques#. Crystal Growth & Design, 2013. **13**(12): p. 5324-5334.
46. Aamir, E., Z. Nagy, and C. Rielly, Evaluation of the effect of seed preparation method on the product crystal size distribution for batch cooling crystallization processes. Crystal Growth & Design, 2010. **10**(11): p. 4728-4740.
47. Aamir, E., Z.K. Nagy, and C.D. Rielly, Optimal seed recipe design for crystal size distribution control for batch cooling crystallisation processes. Chemical Engineering Science, 2010. **65**(11): p. 3602-3614.
48. Ó'Ciardhá, C., N. Mitchell, K. Hutton, and P. Frawley, Determination of the Crystal Growth Rate of Paracetamol As a function of solvent composition. Industrial & Engineering Chemistry Research, 2012. **51**(12): p. 4731-4740.
49. Garside, J., Industrial crystallization from solution. Chemical Engineering Science, 1985. **40**(1): p. 3-26.
50. Abegg, C., J. Stevens, and M. Larson, Crystal size distributions in continuous crystallizers when growth rate is size dependent. AIChE journal, 1968. **14**(1): p. 118-122.
51. Randolph, A. and E. White, Modeling size dispersion in the prediction of crystal-size distribution. Chemical Engineering Science, 1977. **32**(9): p. 1067-1076.
52. Daudey, P.J., Crystallization of ammonium sulfate1987: Ph. D. diss., Delft University of Technology, the Netherlands.

53. Suharso, S., In Situ Measurement of the Growth Rate of the (111) Face of Borax Single Crystal. Jurnal Matematika dan Sains, 2009. **10**(3): p. 101-106.
54. Luo, Y.-H., G.-G. Wu, and B.-W. Sun, Antisolvent Crystallization of Biapenem: Estimation of Growth and Nucleation Kinetics. Journal of Chemical & Engineering Data, 2013. **58**(3): p. 588-597.
55. Dobson, P.S., L.A. Bindley, J.V. Macpherson, and P.R. Unwin, Atomic force microscopy investigation of the mechanism of calcite microcrystal growth under Kitano conditions. Langmuir, 2005. **21**(4): p. 1255-1260.
56. Kuznetsov, Y.G., A. Malkin, and A. McPherson, AFM studies of the nucleation and growth mechanisms of macromolecular crystals. Journal of Crystal Growth, 1999. **196**(2): p. 489-502.
57. Land, T., A. Malkin, Y.G. Kuznetsov, A. McPherson, and J. De Yoreo, Mechanisms of protein crystal growth: an atomic force microscopy study of canavalin crystallization. Physical Review Letters, 1995. **75**(14): p. 2774.
58. Malkin, A.J., T.A. Land, Y.G. Kuznetsov, A. McPherson, and J.J. DeYoreo, Investigation of Virus Crystal Growth Mechanisms by In Situ Atomic Force Microscopy. Physical Review Letters, 1995. **75**(14): p. 2778-2781.
59. McPherson, A., A. Malkin, Y.G. Kuznetsov, and M. Plomp, Atomic force microscopy applications in macromolecular crystallography. Acta Crystallographica Section D: Biological Crystallography, 2001. **57**(8): p. 1053-1060.
60. Shekunov, B.Y. and D.J. Grant, In situ optical interferometric studies of the growth and dissolution behavior of paracetamol (acetaminophen). 1. Growth kinetics. The Journal of Physical Chemistry B, 1997. **101**(20): p. 3973-3979.
61. Shekunov, B.Y., D.J. Grant, R.J. Latham, and J.N. Sherwood, In situ optical interferometric studies of the growth and dissolution behavior of paracetamol (acetaminophen) crystals. 3. Influence of growth in the presence of p-acetoxyacetanilide. The Journal of Physical Chemistry B, 1997. **101**(44): p. 9107-9112.
62. Thompson, C., M.C. Davies, C.J. Roberts, S.J.B. Tendler, and M.J. Wilkinson, The effects of additives on the growth and morphology of paracetamol (acetaminophen) crystals. International Journal of Pharmaceutics, 2004. **280**(1–2): p. 137-150.
63. Vekilov, P.G., M. Ataka, and T. Katsura, Laser Michelson interferometry investigation of protein crystal growth. Journal of Crystal Growth, 1993. **130**(1–2): p. 317-320.
64. Zikic, A., R. Ristic, and J. Sherwood, An instrument for in situ growth rate characterization of mechanically strained crystals. Review of Scientific Instruments, 1998. **69**(7): p. 2713-2719.
65. Liu, B., C.S. Fang, S.L. Wang, and X.M. Mou, In situ measurement of growth kinetics of {100} KDP crystal faces in the presence of polyphosphate impurities. Crystal Research and Technology, 2008. **43**(7): p. 700-708.
66. Li, L. and N. Rodriguez-Hornedo, Growth kinetics and mechanism of glycine crystals. Journal of Crystal Growth, 1992. **121**(1): p. 33-38.
67. Kirkpatrick, R., Crystal growth from the melt: a review. American Mineralogist, 1975. **60**(9-10): p. 798-814.
68. Burton, W.-K., N. Cabrera, and F. Frank, The growth of crystals and the equilibrium structure of their surfaces. Philosophical Transactions of the Royal Society of London. Series A, Mathematical and Physical Sciences, 1951: p. 299-358.

69. Ohara, M. and R.C. Reid, Modeling crystal growth rates from solution. Vol. 225. 1973: Prentice-Hall Englewood Cliffs.
70. Van der Eerden, J., P. Bennema, and T. Cherepanova, Survey of Monte Carlo simulations of crystal surfaces and crystal growth. Progress in Crystal Growth and Characterization, 1978. **1**(3): p. 219-254.
71. Bennema, P.a.v.d.E., J.P., Morphology of crystals1987, Tokyo: Terra Scientific
72. Roberts, K.J., Characterisation and growth mechanisms of flux grown Yttrium Aluminium Garnet. PhD thesis, 1978.
73. Dhanaraj, G., K. Byrappa, and V. Prasad, Springer handbook of crystal growth2010: Springer.
74. Docherty, R., A. El-Korashy, H.-D. Jennissen, H. Klapper, K. Roberts, and T. Scheffen-Lauenroth, Synchrotron Laue topography studies of pseudo-hexagonal twinning. Journal of Applied Crystallography, 1988. **21**(5): p. 406-415.
75. Roberts, K., R. Docherty, P. Bennema, and L. Jetten, The importance of considering growth-induced conformational change in predicting the morphology of benzophenone. Journal of Physics D: Applied Physics, 1993. **26**(8B): p. B7.
76. Billot, P., M. Couty, and P. Hosek, Application of ATR-UV spectroscopy for monitoring the crystallisation of UV absorbing and nonabsorbing molecules. Organic Process Research & Development, 2010. **14**(3): p. 511-523.
77. Kolhe, P., E. Misra, R.M. Kannan, S. Kannan, and M. Lieh-Lai, Drug complexation, in vitro release and cellular entry of dendrimers and hyperbranched polymers. International Journal of Pharmaceutics, 2003. **259**(1): p. 143-160.
78. Docherty, R., K. Roberts, and E. Dowty, MORANG—A computer program designed to aid in the determinations of crystal morphology. Computer Physics Communications, 1988. **51**(3): p. 423-430.
79. Pro, O., 8 (2007). About Origin Pro 8 SRO, V8. 0724 software, Copyright 1991-2007, Origin Lab Corporation.
80. Accelrys, Material Studio
81. Gracin, S. and Å.C. Rasmuson, Solubility of phenylacetic acid, p-hydroxyphenylacetic acid, p-aminophenylacetic acid, p-hydroxybenzoic acid, and ibuprofen in pure solvents. Journal of Chemical & Engineering Data, 2002. **47**(6): p. 1379-1383.
82. Rashid, A., T. White, T. Howes, J. Litster, and I. Marziano, Racemic ibuprofen solubility in ethanol and aqueous ethanolic mixtures. Chemeca 2008: Towards a Sustainable Australasia, 2008: p. 1393.
83. Finnie, S.D., R.I. Ristic, J.N. Sherwood, and A.M. Zikic, Morphological and growth rate distributions of small self-nucleated paracetamol crystals grown from pure aqueous solutions. Journal of Crystal Growth, 1999. **207**(4): p. 308-318.
84. Noyes, A.A. and W.R. Whitney, The rate of solution of solid substances in their own solutions. Journal of the American Chemical Society, 1897. **19**(12): p. 930-934.
85. Ristic, R., S. Finnie, D. Sheen, and J. Sherwood, Macro-and micromorphology of monoclinic paracetamol grown from pure aqueous solution. The Journal of Physical Chemistry B, 2001. **105**(38): p. 9057-9066.
86. Berglund, K. and M. Larson, Modeling of growth rate dispersion of citric acid monohydrate in continuous crystallizers. AIChE journal, 1984. **30**(2): p. 280-287.
87. Berglund, K.A. and V.G. Murphy, Modeling growth rate dispersion in a batch sucrose crystallizer. Industrial & Engineering Chemistry Fundamentals, 1986. **25**(1): p. 174-176.

88. Klug, D.L. and R.L. Pigford, The probability distribution of growth rates of anhydrous sodium sulfate crystals. Industrial & Engineering Chemistry Research, 1989. **28**(11): p. 1718-1725.